In situ studies of morphology, strain, and growth modes of a molecular organic thin film

P. Fenter

Princeton Materials Institute and Department of Physics, Princeton University, Princeton, New Jersey 08540

F. Schreiber

Princeton Materials Institute and Department of Chemistry, Princeton University, Princeton, New Jersey 08540

L. Zhou

Department of Physics, Princeton University, Princeton, New Jersey 08540

P. Eisenberger

Princeton Materials Institute, Princeton University, Princeton, New Jersey 08540
and Lamont Doherty Labs, Columbia University, New York, New York 10027

S. R. Forrest

Princeton Materials Institute, Princeton University, Princeton, New Jersey 08540;
Center for Photonic and Optoelectronic Engineering, Princeton University, Princeton, New Jersey 08540;
and Department of Electrical Engineering, Princeton University, Princeton, New Jersey 08540

(Received 2 April 1997)

We use grazing incidence x-ray scattering to study the molecular structure and morphology of thin (<70 ML) crystalline films of 3,4,9,10-perylenetetracarboxylic dianhydride (PTCDA) on Au(111) surfaces as a function of film thickness, substrate temperature, and growth rate. Although the first two PTCDA monolayers grow in a layer-by-layer fashion, the film evolution beyond the second monolayer depends strongly upon the growth conditions resulting in low-temperature [i.e., nonequilibrium (NEQ)] and high-temperature [equilibrium (EQ)] growth regimes. In the NEQ regime, the films roughen monotonically with increasing film thickness, but retain a well-defined film thickness. Furthermore, we find that these films have a lattice strain which is independent of film thickness. In the EQ regime, the film acquires a three-dimensional morphology for thicknesses >2 ML, and the lattice strain decreases rapidly with increasing thickness. We also show that the transition between the NEQ and EQ regimes is sharp and depends upon the balance between the growth rate and substrate temperature. These results suggest that the PTCDA/Au(111) system is thermodynamically described by incomplete wetting, and that strain and kinetics play an important role in determining molecular organic film characteristics. [S0163-1829(97)09130-3]

I. INTRODUCTION

The growing interest in molecular organic materials as the basis for creating optoelectronic devices (e.g., light emitting diodes[1,2] or waveguide-coupled detectors[3]) has led to an increasing interest in the structure and growth dynamics of organic molecular thin films. Such films hold the promise of a wide tunability in their properties (by making use of the synthetic capabilities of organic chemistry), as well as a high degree of microscopic structural control when grown by the ultrahigh vacuum (UHV) process of organic molecular beam deposition (OMBD), as suggested by the observation of exciton confinement in OMBD grown multiple quantum well structures.[4] This has highlighted the need to understand the structure and morphology of these materials at the molecular level so that the structure-property relationships of these materials can be fully explored. Films consisting of PTCDA (3,4,9,10-perylenetetracarboxylic dianhydride) have been very well studied, and PTCDA is considered to be an archetypal molecular organic thin film material.[5-9] Previous studies have found that uniform crystalline PTCDA films can be grown on a wide range of substrates using OMBD in ultra-high vacuum.[6,9,10] From these observations and the lack of any dislocation defects in thick PTCDA films due to differences in the interlayer and intermolecular binding energies, it has been suggested that molecularly smooth PTCDA films can be grown largely independent of lattice matching conditions, and which has been referred to as ''quasiepitaxy.''[9] Recently, we have determined the two-dimensional (2D) structure of a 17 ML PTCDA film on Au(111) substrates, and found that these films exhibit a finite degree of strain as measured by the aspect ratio of the 2D unit mesh.[11]

More generally, there is wide interest in understanding the behavior of organic/inorganic interfaces, as found in a range of studies from model systems such as self-assembled and Langmuir-Blodgett monolayers and multilayers,[12] to more applied systems such as in the biomineralization of skeletal materials.[13] While these organic/inorganic systems appear very different from the simpler atomic epitaxial systems and also have interactions which are typically weaker (e.g., van der Waals interactions dominate), the degree to which these systems differ in a *fundamental* way from atomic epitaxial systems is not apparent. For instance, there is often little known about the microscopic evolution of the structure and

morphology of organic materials, as compared with what is known about many conventional inorganic film systems (e.g., semiconductors, metals). At present, there is only a limited understanding of the microscopic growth mechanisms of planar organic systems, or even the dependence of the film structure and morphology upon growth conditions. Yet, previous theoretical studies have suggested that large planar molecules (such as PTCDA) should have qualitative differences as compared to other epitaxial systems due to the large mismatch between the molecular size and the substrate lattice spacings as well as the expectation that the substrate-film van der Waals interactions should be relatively low.[14,15]

In the present study, we use grazing incidence x-ray diffraction (GIXD) to study, at the molecular level, the structure and morphology of thin (<70 ML) PTCDA films grown on Au(111) substrates as a function of number of molecular layers, n, substrate temperature, T, and growth rate, R. Au(111) serves as an excellent substrate on which to study the relationship between strain and morphology since the PTCDA/Au(111) bond energy is higher than in previously studied cases of PTCDA on graphite or glass. In the latter situations, it is believed that the weaker film/substrate interaction leads to the growth or relaxed film structures.[9] First, we describe the evolution of the PTCDA film morphology and lattice strain as a function of film thickness for films grown in the low-temperature [or nonequilibrium (NEQ)] growth regime. We then explore the dependence of PTCDA growth on substrate temperature and growth rate to show that there exists a sharp transition between the low-temperature (NEQ) and the high-temperature equilibrium (EQ) growth regimes, and that the transition depends upon both the growth rate and substrate temperature. These results are discussed in the context of previous studies of PTCDA films, and thin film growth in general.

II. EXPERIMENT

The grazing incidence x-ray scattering experiments were performed in an ultrahigh vacuum system which allows for *in situ* analysis of the PTCDA film structure during growth. The Au(111) single crystal substrates are cleaned by sputtering and annealing, resulting in the expected $\sqrt{3} \times 23$ surface reconstruction,[16] and the PTCDA films are grown on Au(111) single crystalline surfaces by OMBD. The PTCDA source is a resistively heated tantalum oven with a small (~ 1 mm^2) aperture covered with a fine tungsten mesh. The x-ray scattering measurements were performed at the Exxon X10B beamline at the National Synchrotron Light Source. In these measurements, the radial resolution of 0.008 Å^{-1} is set by slits before the detector, corresponding to a resolution limit of ~ 800 Å (none of the reported data are limited by the x-ray resolution). The PTCDA beam flux during growth was independently monitored using a quartz crystal microbalance (QCM), and was calibrated through the observation of oscillations in the specular x-ray intensity as a function of time during the growth, due to the subsequent addition of each monolayer.[17] We note that there is a discrepancy between the PTCDA *flux* (as derived from QCM) and the PTCDA *coverage* (as derived by the x-ray intensity analysis and described in Sec. III). In general, a smaller coverage is derived from the x-ray intensity analysis than is found by monitoring the
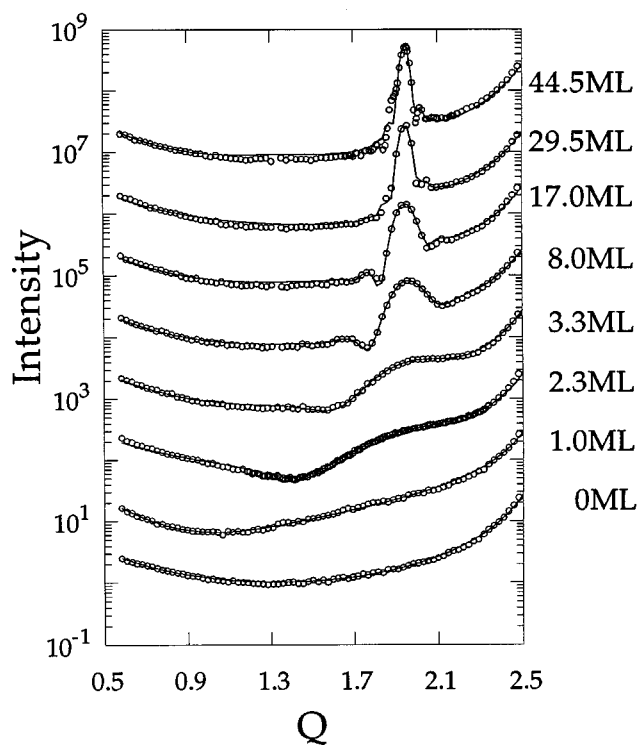

FIG. 1. Specular reflectivity (circles) of PTCDA/Au(111) is shown as a function of the PTCDA film thickness (shown in units of PTCDA monolayers, in which 1 ML corresponds to 3.22 Å). The solid line is a fit to the data assuming a density profile of the form of Eq. (1). All films were grown at a substrate temperature of 17 °C, except the 1.0 and 2.3 ML films which were grown at 100 °C. The growth rate for these films was ~ 5 ML/min, except the 1, 2.3, and 29.5 ML samples which were grown at a rate of ~ 0.8 ML/min. Each set of data is vertically offset by a factor of 10 for clarity.

PTCDA flux with the QCM, suggesting that the sticking coefficient may decrease after completion of the first two monolayers (which were used for the QCM calibration). For simplicity, all film thicknesses quoted in this work are derived from the QCM reading.

III. RESULTS

A. Film evolution vs thickness (NEQ regime)

In Fig. 1, we show the evolution of the wide angle x-ray specular reflectivity[18] for a clean Au(111) surface, and as a function of film thickness ranging from 1 ML up to ~ 45 ML of PTCDA. These data show the Au crystal truncation rod, exhibiting a $\sin^{-2}(Qd_{111}/2)$ functional form, where the momentum transfer, Q, is related to the scattering angle, 2θ, by the relation $Q = (4\pi/\lambda)\sin(2\theta/2)$. Here, λ is the x-ray wavelength, and $d_{111} = 2.356$ Å is the d-spacing for the (111) Bragg planes of the Au substrate. The PTCDA ($1\,0\,2$) Bragg peak is found at $Q = 1.95$ Å^{-1} corresponding to $d_{102} = 3.22$ Å. The ($1\,0\,2$) Bragg peak becomes both more intense and narrower as the film thickness is increased, as expected for the growth of a well ordered crystal. As we have previously observed,[11] the data for the thicker films exhibit oscillations of the intensity above and below the ($1\,0\,2$) Bragg peak, indicating that there exists a well defined film thickness, although the rapid damping of these oscillations away from the

(1 0 2) Bragg peak indicates that the film thickness is not uniform on a molecular (i.e., one monolayer) scale.

The (1 0 2) Bragg peak is accurately aligned along the Au(111) substrate surface normal, with no evidence for any extra mosiac (angular) broadening. Therefore, we infer that the PTCDA molecules form well-defined lamella parallel to the Au substrate surface. Furthermore, we have no evidence of any stacking disorder in these films, or even any out-of-plane orientational disorder (i.e., mosaic about the surface normal). Consequently, understanding the PTCDA film structure along the surface normal reduces to a determination of the occupation of each molecular layer (i.e., the PTCDA density profile). This can be determined by comparing the x-ray reflectivity data to a model in which the density of each PTCDA layer is allowed to vary. Since the x-ray scattering data in Fig. 1 are in the ''large angle'' regime, they are sensitive to the density and spacings of the crystalline

PTCDA film at the level of the PTCDA layer spacing, d_{102} = 3.22 Å. This is distinct from the density profile determined from a small angle reflectivity, which is sensitive only to the total density distribution independent of the degree of order and/or crystallinity.

We model the PTCDA density profile, $\rho(n)$, with a phenomenological expression which has three characteristics: (1) An arbitrary layer density, $\rho(n)$, for the first three PTCDA layers ($n \leq 3$) which allows for the possibility of a different 2D structure (and therefore different 2D density) in the first few layers due to the PTCDA/Au interaction, (2) an exponential decay of the density for $n > 3$, with an asymptotic limit of ρ_N (the layer density near the film surface) with a decay length, L, and (3) a density cutoff (at layer N) having a root-mean-square (rms) roughness, ΔN. An empirical expression which contains each of these characteristics can be written (for $n \geq 3$) as

$$\rho(n) = [(\rho(3) - \rho_N)\exp(-(n-3)/L) + \rho_N]/[1 + \exp(1.59(n-N)/\Delta N)]. \qquad (1)$$

We have chosen this functional form since Eq. (1) provides a flexible functional form capable of reproducing a wide range of possible density profiles, ranging from an ideal step function (with no surface roughness) to a monotonically decreasing density profile characteristic of a three-dimensional (3D) film morphology. Furthermore, Eq. (1) can quantitatively reproduce the x-ray scattering intensities of PTCDA films grown under a wide range of conditions. By integrating the derived density profile, we can obtain the adsorbed mass of the film.[19] In order to calculate the scattering intensity of this film, we must also include the specular reflectivity of the semi-infinite Au(111) substrate (as indicated in the 0 ML curve in Fig. 1), which results in the $\sin^{-2}(Qd_{111}/2)$ dependence found for the clean surface.

The calculated scattering intensities for the best fit density profiles are shown as solid lines in Fig. 1. Note that the calculations using Eq. (1) fit both the changes in the (1 0 2) peak shape as a function of thickness, as well as the damping of the intensity oscillations away from the (1 0 2) peak position for film thicknesses of up to ~30 ML. For the 44.5 ML film, we are unable to quantitatively explain the x-ray intensities within this model, which suggests that actual density profile for thicknesses of >30 ML is no longer adequately described by Eq. (1).

In Fig. 2, we show the derived density profiles, which plot the film density as a function of the molecular layer number, n. In these plots, the density of bulk PTCDA is normalized to $\rho = 1.0$. These density profiles have two characteristics: there is a broad termination of the film density at the PTCDA film surface (for thicknesses greater than 2 ML), and the film density decreases continuously within the film. To test the uniqueness of these results, we have also fit the data (for relatively thin films, $N \leq 15$ ML) by allowing the density of each layer to vary as an independent parameter. While the derived density profiles are noisy (as expected since the number of independent fitting parameters is larger than is

justified by the data), they had all of the same features found in the density profiles in Fig. 2 using the phenomenological fit based upon Eq. (1).

We now address the evolution of the rms surface roughness, ΔN, which is plotted in Fig. 3 as a function of film thickness. At the initial stage of growth, the first and second monolayers appear to completely cover the Au surface before any additional layers are occupied (i.e., the first two monolayers ''wet'' the Au surface); this is supported by our observation of layer-by-layer intensity oscillations during the growth at the PTCDA anti-Bragg condition for only the first two monolayers,[17] as well as our observation that these layers are more strongly bound to the Au(111) surface than found in bulk PTCDA. For instance, while ''bulk'' desorption from a multilayer PTCDA film occurs at ~240 °C, we
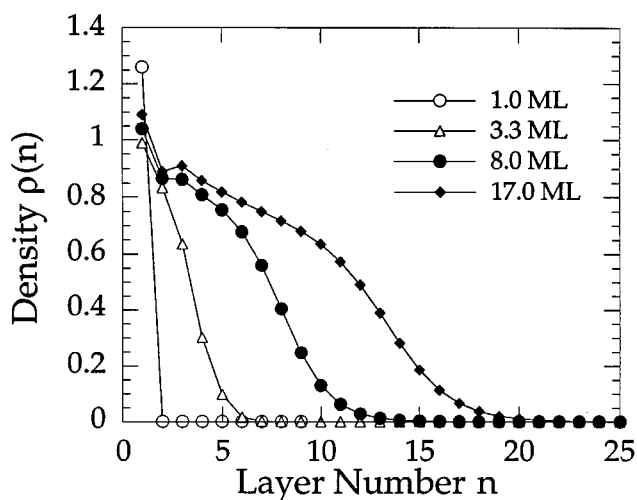

FIG. 2. The derived density profiles as a function of the PTCDA film thickness for the x-ray scattering data shown in Fig. 1. The film thicknesses are noted, and the growth conditions are specified in Fig. 1.
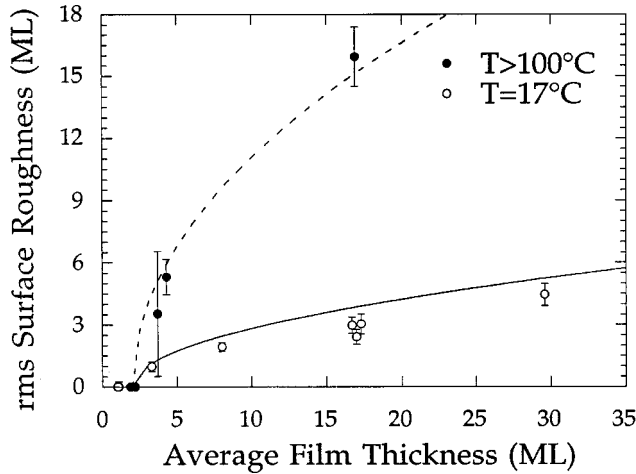
FIG. 3. The measured rms surface roughness as a function of film thickness, for substrate temperatures of $T = 17\,°C$ (NEQ regime, open circles) and $T \geq 100\,°C$ (EQ regime, closed circles). The solid line is the expected evolution for random deposition, which has been offset by 2 ML to take into account the wetting layer; the dashed line is a guide to the eye for data in the EQ regime.

find that a bilayer of PTCDA is stable for $240\,°C < T < 250\,°C$, and that a monolayer is stable for $250\,°C < T < 400\,°C$. We have also found that the coverage in the presence of a PTCDA flux can be thermodynamically controlled at the monolayer and bilayer level by varying the substrate temperature, but that below $240\,°C$ the film thickness is controlled kinetically as a function of the incident flux. In the second stage of growth, the third and subsequent layers do not appear sequentially but instead form a growth front which roughens monotonically with increasing film thickness. For example, we find that an average ~ 3.3 ML thick film has a nonzero layer occupation for up to 5 distinct layers.

In order to quantitatively understand the evolution of NEQ film growth, the surface roughness is plotted as a function of the total adsorbed mass (as measured by the QCM) in Fig. 3. We also compare these data to a simple kinetic roughening model[20] in which the molecules randomly adsorb without any surface diffusion. In this model, the rms surface roughness increases as the square root of the film thickness, shown by the solid line in Fig. 3 (offset to account for the 2 ML wetting film), and provides a reasonable description of the evolution of surface roughness to thicknesses as high as ~ 30 ML.

Next, we address the density gradient within the interior of the film, which is clearly observed in Fig. 2. Although the surface roughening is well described by random adsorption, the observed density gradient within the film is not a characteristic of this model. By approximating the density profile if Eq. (1) with a linear slope, we find that the normalized density gradient is $(1/\rho)d\rho/dn = -(\rho(3) - \rho_N)/L$. Then for the 17 ML film in Figs. 1 and 2, the density gradient is determined to be $(1/\rho)d\rho/dn = -0.034 \pm 0.013$, which is a statistically significant deviation from the expected flat density profile. The physical significance of the density gradient is that the completion of each layer (for $n > 2$) is inhibited, resulting in a quasi-three-dimensional film morphology.

To further understand this roughening, we have obtained

atomic force microscope (AFM) images of a 16.5 ML film grown under similar conditions. The AFM images reveal a "mesa"-like microstructure, with a typical mesa having a diameter of ~ 4000 Å, and where each mesa is separated by "valleys." Furthermore, the images show that the mesas have molecularly flat surfaces, and in many cases individual steps having the expected PTCDA layer spacing (3.22 Å) can be observed. These observations suggest that the density gradient in Fig. 2 is due to the valleys between the mesas, and that the *surface* roughness (which in our analysis is independent of the *morphological* roughness due to the valleys) appears to be due to a distribution of mesa heights, as opposed to a random roughness at the molecular scale.

B. Strain evolution vs film thickness (NEQ regime)

Previous studies of thick (0.4 μm) PTCDA films grown in the NEQ regime indicate uniform films without any evidence of islanding,[9] they were performed on amorphous substrates or on graphite. Furthermore, studies of ~ 300 Å thick PTCDA films on oxidized silicon wafers did not find any evidence for islanding.[6] This suggests that the difference between these earlier results and for PTCDA/Au(111) discussed here lies in the nature of the substrate surface and the strength of the molecule/substrate bond.[14,15] We have previously found that PTCDA films grown on Au(111) surfaces have a preferred 2D orientational alignment with the substrate, and have a large (4%) 2D lattice strain[11] even though the PTCDA films are incommensurate with the substrate lattice spacings by 2%.[11] Both of these observations imply that the interaction between the PTCDA film and the Au(111) substrate is stronger than for these previously studied systems. We therefore have extended our investigation to investigate how strain evolves as a function of thickness, and determined its relationship to the observed film morphology.

A schematic of the 2D structure of PTCDA/Au(111) in both real and reciprocal space is shown in Figs. 4(a) and 4(b). Using x-ray diffraction, we show wide angle azimuthal scans through the (0 1 2) Bragg peaks in Fig. 5. From the multiplicity of diffraction peaks, it is evident that there exists more than one orientation of the PTCDA film with respect to the Au substrate. This is in contrast to our previously published data which showed only one 2D orientation with respect to the substrate lattice.[11] We have found that the number of inequivalent film orientations depends upon the details of the Au substrate (e.g., surface miscut) and the growth conditions used. For instance, the orientation of PTCDA films on a graphite surface was found to be affected by the orientation of step edges.[21] Some of the variability between substrates may be explained by the detailed nature of the Au surface such as the magnitude and direction of the surface miscut.

A PTCDA film having a particular orientation (with its symmetry equivalent orientations separated by 60°) would exhibit both (0 1 2) and (0 1 -2) Bragg peaks, having an azimuthal separation, $\Delta\phi$, determined by the 2D PTCDA lattice spacings (a, b). That is

$$\Delta\phi = \phi_{012} - \phi_{01\text{-}2} = 2\arctan(2b^*/a^*) = 2\arctan(2a/b),$$

(2)

(a)

(0,1,2)

(0,1,-2)
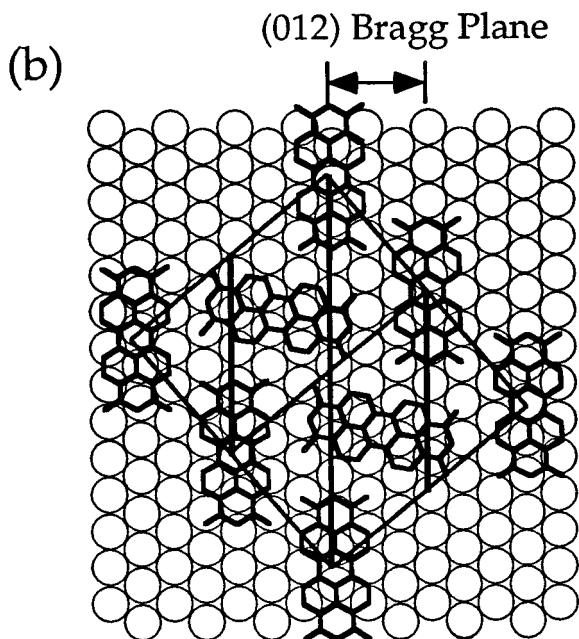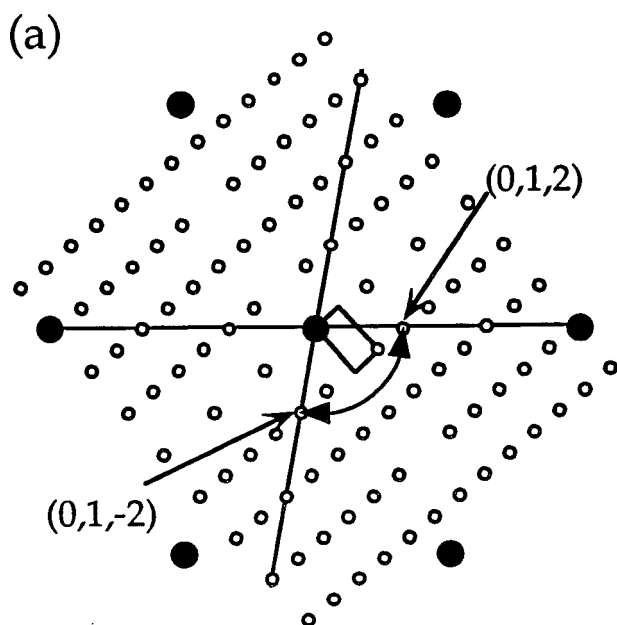
(b)

(012) Bragg Plane

FIG. 4. A 2D schematic of the (a) reciprocal and (b) real space structure of a PTCDA film on a Au(111) substrate. The open circles in (a) are diffraction peaks due to the PTCDA film with the (0 1 2) Bragg peak noted, while the filled circles are Bragg peaks due to the Au(111) surface. In (b), the (0 1 2) Bragg plane is shown for the film orientation which is aligned along the $\phi=0°$ azimuth.

where a^* and b^* are the reciprocal lattice vectors corresponding to the (0 1 0) and (0 0 1) Bragg peaks (e.g., $a^* = 2\pi/a$), respectively. For an unstrained PTCDA lattice, the unit mesh has dimensions[22] of $(a,b) = (11.96$ Å, 19.91 Å) with $a/b = 0.6007$, corresponding to a peak separation of $\Delta\phi = 100.5°$. Given the six-fold symmetry of the Au substrate, this results in an azimuthal peak separation of 19.5°. Therefore, an unstrained PTCDA film aligned along the $\phi=0°$ azimuth would exhibit (0 1 2) Bragg peaks at $\phi=0°$, and (0 1 -2) Bragg peaks at $\phi=19.5°$ and 40.5° (as well as symmetry equivalent orientations separated by 60°). Conse-
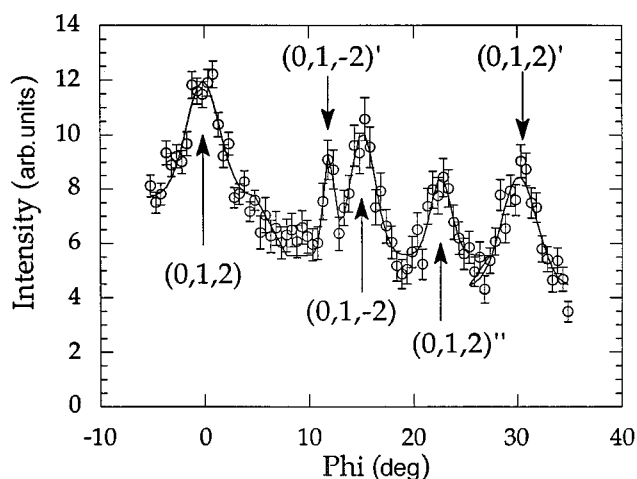

FIG. 5. A wide angle azimuthal scan through the (0 1 2) Bragg peaks of the same 3.3 ML film shown in Fig. 1(a). The contributions from three distinct film orientations, $(0,1,\pm2)$, $(0,1,\pm2)'$, and $(0,1,\pm2)''$, are clearly apparent.

quently, while the (0 1 2) and (0 1 -2) Bragg peaks are equivalent with respect to the film, they have inequivalent orientations with respect to the Au substrate.

Based upon these arguments, we can assign each of the Bragg peaks to a particular PTCDA film orientation. For instance, the peaks labeled (0 1 2) and (0 1 -2) are due to a PTCDA film orientation defined by the alignment of the (0 1 2) Bragg peak along the $\phi=0°$ axis of the Au substrate [as shown in Figs. 4(a) and 4(b)]. Similarly, a second film orientation is defined by the alignment of the (0 1 2)' peak along the $\phi=30°$ direction, and a third domain (0 1 2)'' is aligned along a low symmetry direction. Due to the number of inequivalent domains, we have also confirmed these assignments by measuring the separation of the (0 1 1) and (0 1 -1) Bragg peaks, which provides an independent determination of the film orientation.

Using Eq. (2), we can determine the aspect ratio of the PTCDA unit cell through a measurement of the azimuthal separation of the (0 1 2) and (0 1 -2) Bragg peaks. In Fig. 5, we show data for a 3.3 ML film grown at 17 °C and a growth rate of 3.9 ML/min. The observed peak separation for the $\phi=0°$ orientation, $\Delta\phi = 15.2\pm0.3°$, is significantly smaller than the expected value of 19.5°, which corresponds to an aspect ratio of $a/b = 0.649\pm0.003$. If we define the film strain, δ, as the fractional deviation of the unit cell aspect ratio from the expected bulk value, then $\delta = [(a/b)_{film} - (a/b)_{bulk}]/(a/b)_{bulk} = 0.08$, where $(a/b)_{bulk} = 0.6007$. In the context of inorganic growth, 8% strain would be considered very large, although it is of a similar magnitude to that which we have measured for other organic thin film systems, such as self-assembled monolayers.[23] Similarly, the aspect ratio for the $\phi=30°$ domain is found to be $a/b = 0.615 \pm 0.003$, corresponding to a strain of $\delta=0.024$. The dependence of the lattice strain upon the azimuthal orientation with respect to the *same* substrate clearly demonstrates the sensitivity of the film strain to the *atomic* scale structure and symmetry of the substrate lattice.

In Fig. 6(a), we plot the lattice strain as a function of film thickness for films grown under nonequilibrium (i.e., NEQ) conditions. Although δ is relatively large [~7% and ~4%

for the $(0\,1\,2)$ and $(0\,1\,2)'$ domains], there does not appear to be any systematic decrease of the strain (i.e., strain relief) even for film thicknesses of up to ~70 ML (>200 Å). This implies either that the critical thickness of the PTCDA film is very large, or that the kinetic barrier to relieve the strain is sufficiently high that the strain is frozen-in at room temperature. Note that this lack of strain relief is consistent with previous fluorescence studies of PTCDA/NTCDA multilayer structures grown under similar (NEQ) conditions. There it was found that the exciton-phonon coupling, a property expected to be very sensitive to strain, did not change as the PTCDA layer thickness was increased from 10 to 500 Å.[24]

C. Transition from NEQ to EQ growth regimes

To understand the influence of diffusion in the observed morphologies and the degree to which they represent equilibrium structures, we now discuss the dependence of the film morphology on the substrate temperature during growth. In Fig. 3, we compare the evolution of the film surface width for films grown at high temperature ($T \gtrsim 100$ °C) to films grown at 17 °C. Although we have found layer-by-layer growth for the first two monolayers independent of the substrate temperature (for temperatures as high as 180 °C), there is a significant difference in the film evolution between these two temperature ranges. While films grown at NEQ indicate a slow, monotonic evolution of the surface roughness, films grown at high temperature exhibit a much stronger divergence of the surface roughness for thicknesses >2 ML. The sudden increase of the surface roughness (particularly under equilibrium conditions) coupled with the two stage growth behavior, indicates that the equilibrium film morphology of the PTCDA/Au(111) system corresponds to incomplete wetting.

In Fig. 6(b), the measured 2D lattice strain is shown as a function of thickness for films grown at substrate temperatures of $T > 100$ °C, and growth rates of $R \sim 0.8$ ML/min (i.e., within the EQ regime). These data indicate that the strain for films of a few monolayers thickness is very similar to that found for the nonequilibrium films, although the strain is nearly completely relieved for film thicknesses exceeding ~15 ML. This implies that the observed changes in film morphology and lattice strain are correlated, and that both are determined by the growth regime.

To understand the nature of the transition between the NEQ and EQ regimes, in Fig. 7 we show the evolution of the wide angle x-ray specular reflectivity for a series of 17 ML films grown at $R = 6.7$ ML/min, as a function of the substrate temperature during growth. These data demonstrate that, for $T \lesssim 110$ °C, the films exhibit a temperature independent morphology (similar to that shown in Figs. 1 and 2), but for $T > 110$ °C there is a significant change in the film morphology as indicated by the sudden loss of the intensity oscillations near the $(1\,0\,2)$ Bragg peak. A plot of the surface roughness vs temperature for these films (Fig. 8) shows that this transition is associated with an abrupt increase in the film surface roughness. Qualitatively, this appears to be due to the formation of large 3D islands as the film evolves towards the equilibrium incomplete wetting morphology. The evolution in the surface width vs temperature for a lower growth rate of 0.6 ML/min is also shown in Fig. 8. While the roughness in
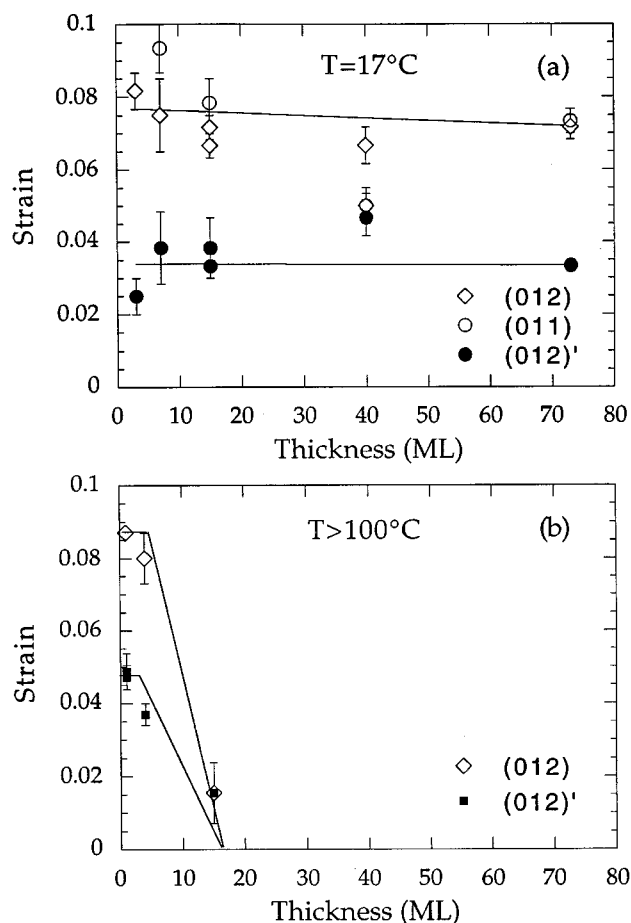

FIG. 6. A plot of the measured lattice strain, defined as the fractional deviation of the (a/b) ratio from the bulk value, as a function of PTCDA film thickness, plotted for (a) the NEQ regime ($T = 17$ °C, and growth rate of ~4 ML/min), and (b) the EQ regime (the 4.4 and 17.3 ML samples were grown at $T = 170$ °C, while the 1 ML sample was grown at 100 °C, and the growth rate was 0.8 ML/min). In (a), the lattice strain for the $(0\,1\,2)$ domain is derived independently through the separation of both the $(0,1,\pm 2)$ and $(0,1,\pm 1)$ Bragg peaks. There is no significant decrease in the lattice strain as a function of film thickness for NEQ films, in contrast to the strong decrease in strain for films grown in the EQ regime.

the NEQ regime is indistinguishable from that found at higher growth rates, the transition temperature between NEQ and EQ regimes decreases by ~40 °C when the growth rate is reduced by an order of magnitude. This demonstrates that the film morphology near the transition between equilibrium and nonequilibrium growth regimes results from a balance between adsorption and diffusion, while the film morphology appears to be independent of the growth rate and substrate temperature within the NEQ regime.

To further probe the mechanisms involved in the transition between NEQ and EQ regimes, we note that films grown at NEQ do not undergo a transition to the EQ morphology when annealed at temperatures as high as 100 °C. In fact, these films actually exhibit an *increase* in the number of intensity oscillations near the $(1\,0\,2)$ Bragg peak for annealing times of up to many hours (as compared to the loss of intensity oscillations for films *grown* at these temperatures). Therefore the transition towards a 3D morphology is not due simply to thermally activated molecular diffusion at these
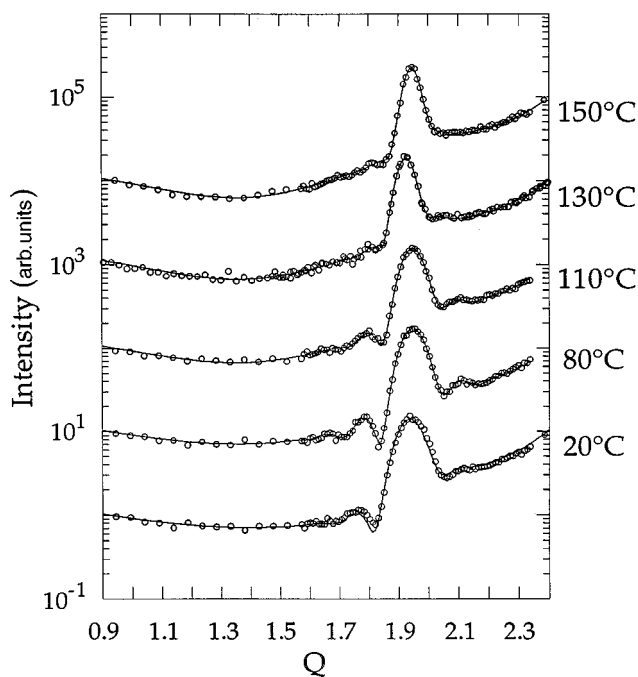
FIG. 7. Specular x-ray reflectivity (circles) of a series of PTCDA films on Au(111) as a function of the substrate temperature during growth for 17 ML PTCDA films. The growth rate was 0.6 ML/min. The solid line is a fit to the data as described in the text.

temperatures, but instead appears to be due to a dynamical aspect of the growth process itself. Since the resulting film morphology is typically a result of a balance between the adsorption and diffusion rates, this suggests that the diffusion is strongly modified *during growth*. This may be due to a transient mobility of the PTCDA molecules upon adsorption[25] (in which the latent heat of adsorption may be converted, at least in part, to kinetic energy).

Given the observed ''mesa'' morphology in NEQ grown film, the sharpness of the transition between low- and high-temperature regimes suggests that the evolution towards a
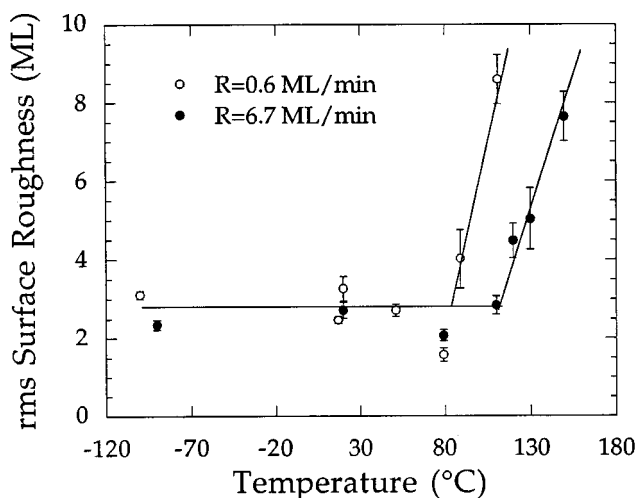

FIG. 8. Film surface roughness of a 17 ML film as a function of substrate temperature, for growth rates of $R = 0.6$ ML/min (open circles) and $R = 6.7$ ML/min (filled circles). Note that the crossover temperature between the NEQ and EQ regimes increases substantially as R increases.

3D morphology may be possible when the diffusion length of the molecules is larger than the average mesa size. Under such conditions, the film may undergo Ostwald ripening[26] (but by making use of transient mobility instead of thermally activated diffusion) in which larger islands grow at the expense of the smaller ones, resulting in a 3D island morphology in the EQ regime. In contrast, when the diffusion length is smaller than the size of a typical mesa, we expect that temperature independent NEQ film morphology will be found.

IV. DISCUSSION AND CONCLUSIONS

These results provide a detailed picture of the structure and morphology of PTCDA films grown on single crystalline Au(111) substrates, and demonstrate that the evolution of molecular organic film growth can be unexpectedly complex, particularly in cases where there is a relatively strong molecule/substrate interaction.[14,15] We have found that in the low-temperature (NEQ) regime, PTCDA films exhibit a ''mesa'' morphology, and that these films also have a large ($\sim 8\%$) lattice strain as exhibited as a change in the a/b ratio of the 2D unit mesh. This lattice strain does not decay with increasing film thickness. When grown in the high-temperature (EQ) regime, a 3D film morphology is observed, and the lattice strain decreases rapidly for increasing film thicknesses. These observations suggest that PTCDA incompletely wets the Au(111) surface, and that lattice strain is likely to be the driving force for the mesa morphology found in the NEQ regime.

We have also found that the transition between the NEQ and EQ regimes is sharp, and depends upon both the substrate temperature and growth rate. We also observe that we cannot transform films grown in the NEQ regime to an EQ morphology simply by annealing the film at substrate temperatures which correspond to the EQ regime. This suggests that this transition is a dynamical phenomenon due to a balance between the adsorption and diffusion rates during the growth process.

It is useful to compare these results with low-temperature studies (<60 K) of simple molecular systems which have previously been the subject of considerable study. In these systems (such as Xe, Ar, N_2, and Ne films adsorbed on graphite[27]) it has been found that true layer-by-layer growth (i.e., wetting) exists when the ratio of the molecule-substrate to molecule-molecule interactions is minimal, while incomplete wetting occurs when this ratio is large. This point of view has also been supported by theoretical studies[28] which show that stresses imposed by the substrate will result in a strain field within the film, and induce incomplete wetting. This appears to be consistent with our observations that the PTCDA-Au interaction is stronger than the PTCDA-PTCDA interaction, which presumably induces the observed lattice strain, and results in incomplete wetting. Further, we note that unstrained incommensurate ''quasi-epitaxial'' systems have been predicted and observed for small PTCDA/substrate interactions. We view the PTCDA/Au(111) system grown at NEQ conditions bears many similarities to these so-called ''quasiepitaxial'' systems, but can also be understood in the context of highly strained epitaxial film growth.

What is perhaps most unusual is the kinetic aspect of the

PTCDA/Au(111) system. We have found that the NEQ film morphology is apparently independent of the substrate temperature during growth from as low as $-100\,°C$ to as high as $\sim100\,°C$, and that the observed lattice strain does not decay for film thicknesses as high as 70 ML. Once grown, these films are stable, even when annealed at temperatures corresponding to 3D *growth* conditions. Together these results suggest that the energetic barrier for fundamental processes (such as molecular diffusion) is apparently sufficiently high so as to limit any thermally induced evolution of the film structure and morphology.

Note added in proof. Multiple orientations of PTCDA/Au(111) (see Sec. III B) have recently been observed by STM by Schmitz-Hübsch *et al.* [Phys. Rev. B **55**, 7972 (1997)].

[1] C. W. Tang and S. A. VanSlyke, Appl. Phys. Lett. **51**, 913 (1987).

[2] P. E. Burrows and S. R. Forrest, Appl. Phys. Lett. **62**, 3102 (1993).

[3] R. B. Taylor, P. E. Burrows, and S. R. Forrest, IEEE Photonics Technol. Lett. **9**, 365 (1997).

[4] F. F. So and S. R. Forrest, Phys. Rev. Lett. **66**, 2649 (1991).

[5] M. Möbus, N. Karl, and T. Kobayashi, J. Cryst. Growth **116**, 495 (1992).

[6] M. Möbus and N. Karl, Thin Solid Films **215**, 213 (1992).

[7] C. Ludwig, B. Gomph, W. Glatz, J. Petersen, W. Eisenmenger, M. Mobus, U. Zimmerman, and N. Karl, Z. Phys. B **86**, 397 (1992).

[8] F. F. So and S. R. Forrest, Mol. Cryst. Liq. Cryst. Sci. Technol. **2**, 205 (1992).

[9] S. R. Forrest, P. E. Burrows, E. I. Haskal, and F. F. So, Phys. Rev. B **49**, 11 309 (1994).

[10] H. Fuchigami, S. Tanimura, Y. Uehara, T. Kurata, and S. Tsunoda, Jpn. J. Appl. Phys. 1 **34**, 3852 (1996).

[11] P. Fenter, P. Burrows, P. Eisenberger, and S. R. Forrest, J. Cryst. Growth **152**, 65 (1995).

[12] A. Ulman, *An Introduction to Organic Thin Films* (Academic, San Diego, 1991).

[13] S. Mann, D D. Archibald, J. M. Didymus, T. Douglas, B. R. Heywood, F. C. Meldrum, and N. J. Reeves, Science **261**, 1286 (1993).

[14] S. R. Forrest and Y. Zhang, Phys. Rev. B **49**, 11 297 (1994).

[15] Y. Zhang and S. R. Forrest, Phys. Rev. Lett. **71**, 2765 (1993).

[16] A. R. Sandy, S. G. J. Mochrie, D. M. Zehner, K. G. Huang, and D. Gibbs, Phys. Rev. B **43**, 4667 (1991).

[17] P. Fenter, P. Eisenberger, P. Burrows, S. R. Forrest, and K. S. Liang, Physica B **221**, 145 (1996).

[18] I. M. Tidswell, B. M. Ocko, P. S. Pershan, S. R. Wasserman, G. M. Whitesides, and J. D. Axe, Phys. Rev. B **41**, 1111 (1990).

[19] We have assumed in this analysis that the PTCDA molecules are flat, that thermal vibrations are negligible, and that there is minimal inhomogeneity of the stacking of the molecules; deviations from these assumptions will reduce the derived density of an ideal PTCDA layer density. From a comparison of the $(1\,0\,2)$ and (204) Bragg peaks, we have found that these assumptions are justified since the combination of static and dynamic Debye-Waller contributions at room temperature is $u\sim0.1$ Å (u is the mean square deviation from the equilibrium position), which reduces the coherent scattering intensity of the PTCDA film at the $(1\,0\,2)$ Bragg peak by only $\sim4\%$.

[20] P. I. Cohen, G. S. Petrich, P. R. Pukite, G. J. Whaley, and A. S. Arrott, Surf. Sci. **216**, 222 (1989).

[21] C. Kendrick, A. Kahn, and S. R. Forrest, Appl. Surf. Sci. **104/105**, 586 (1996).

[22] A. J. Lovinger, S. R. Forrest, M. L. Kaplan, P. H. Schmidt, and T. Venkatesan, J. Appl. Phys. **55**, 476 (1984).

[23] P. Fenter, A. Eberhardt, K. S. Liang, and P. Eisenberger, J. Chem. Phys. **106**, 1600 (1997).

[24] E. I. Haskal, Z. Shen, P. E. Burrows, and S. R. Forrest, Phys. Rev. B **51**, 4449 (1995).

[25] W. F. Egelhoff and I. J. Jacobs, Phys. Rev. Lett. **62**, 921 (1989).

[26] M. Zinke-Allmang, L. C. Feldman, and L. C. Grabow, Surf. Sci. Rep. **16**, 378 (1992).

[27] J. L. Seguin, J. Suzanne, M. Bienfait, J. G. Dash, and J. A. Venables, Phys. Rev. Lett. **51**, 122 (1983).

[28] D. A. Huse, Phys. Rev. B **29**, 6985 (1984).